RESEARCH PAPER
PCCP
www.rsc.org/pccp

The significance of electrokinetic characterization for interpreting interfacial phenomena at planar, macroscopic interfaces

Keqing Fa,*[ab] Vamsi K. Paruchuri,[a] Scott C. Brown,[c] Brij M. Moudgil[c] and Jan D. Miller[a]

[a] *Department of Metallurgical Engineering, University of Utah, 135 South 1460 East, Salt Lake City, UT 84112, USA. Fax: 801 581 4973; Tel: 801-581 5160*
[b] *Department of Chemistry and Beckman Institute for Advanced Science and Technology, University of Illinois at Urbana-Champaign, 405 N Mathews, Urbana, IL 61801, USA. E-mail: kfa@uiuc.edu; Fax: 217 244 0181; Tel: 217 244 5767*
[c] *Particle Engineering Research Center, University of Florida, Gainesville, FL 32611, USA*

Received 26th November 2004, Accepted 6th January 2005
First published as an Advance Article on the web 17th January 2005

Streaming potential measurements provide valuable information for the validation and interpretation of interfacial phenomena that occur at flat macroscopic surfaces. Planar substrates have been extensively used for the interpretation of events, which occur at particulate surfaces; however, these flat surfaces are often only questionably representative of their particulate counterparts due to variations in surface chemistry and topography. In this study, the zeta potential from planar macroscopic surfaces of PMMA, mica, graphite, fluorite, and calcite have been calculated from streaming potentials measured in aqueous solutions using an asymmetric clamping cell. These zeta potentials have been found to significantly contribute to understanding and interpretation of interfacial phenomena influenced by Coulombic interactions including adsorption, surface forces, and the structure of surface micelles.

Introduction

The importance of surface charge in understanding interfacial phenomena such as adsorption,[1–3] crystallization, and coagulation/dispersion has been well established for many systems.[1] The zeta potential, formally defined as the electric potential at the plane of shear in the electric double layer structure, provides considerable insights regarding the charging behavior of solid surfaces and colloidal particles immersed in aqueous solutions.

Surface charge at mineral surfaces can be generated by one or more mechanisms such as dissociation of surface acid groups,[4–6] lattice substitution,[7–9] and preferential hydration of surface lattice ions.[10–12] In some cases, a surface may be charged by the orientation of dipoles or by surface polarization.

There are four fundamental methods used to determine the zeta potential. These methods include the measurements of streaming potential, sedimentation potential, electro-osmosis, and electrophoresis. Of these, electrophoresis measurements are mainly used to determine the zeta potential of particles. The electrophoretic mobility measured is converted to the zeta potential value generally based on the Henry or Smoluchowski approximation.[13] There are several reported theories and experimental procedures for obtaining the zeta potential at flat plates using the streaming potential measurement technique.[14–22] Traditionally, the streaming potential technique is often applied to membranes and thin films because the membrane and thin film surfaces are smooth and of sufficient size to form the desired measuring channels. Recently, the advent of an asymmetric clamping cell[14] promotes research for streaming potential measurement of flat plates by circumventing the requirements that the flat plate samples must be easy to cut and drill, and be of sufficient dimensions.

A laminar flow at steady state is required to calculate zeta potentials from streaming potential. For smooth flat plates, the traditional Helmholtz–Smoluchowski approach is applied. For the porous membrane, an additional term is necessary to describe the wall effect.[20–22] It has been found that the zeta potential calculated from the streaming potential measurement is generally lower than that obtained from the electrophoretic mobility measurement[23–25] and the magnitude of the zeta potential varies with change in the background electrolyte solution[26–28] and the operating mode.

Interfacial phenomena are often probed on a more fundamental level through modern diagnostic tools such as AFM, surface spectroscopy (FTIR, SFG), *etc.*, in which case flat surfaces frequently are required for study rather than particles. Some ambiguity may exist when electrophoretic mobility data are used to explain surface force measurements and surface spectroscopy analysis of planar surfaces.[29–30] Because the surfaces of a small particle are not defined with respect to a specific crystallographic orientation, the exposed surface atoms with different orientations are not necessarily the same. The zeta potentials measured using mineral particles can be significantly different from those measured using a flat mineral plate with a specific crystallographic orientation.[31] For example, it was reported that the IEP of sapphire single crystals was between pH 5.0 and pH 6.0 while the IEP of alpha alumina powder was found to be pH 9.0.[31] In this regard, streaming potential measurements for the flat plate geometry would be more appropriate for zeta potential determination in some studies. In this paper we report zeta potential calculation for flat surfaces as determined from streaming potential measurements for some selected systems using a novel asymmetric clamping cell and compare the calculated flat plate zeta potentials with those calculated from particle electrophoretic mobility measurements. The significance of these results is discussed with respect to various observations made from AFM and surface spectroscopy experiments.

Experimental

Materials

High purity Milli-Q water (+18 MΩ cm) was used throughout the experiments.

DOI: 10.1039/b417902a

Calcium dioleate spheres were prepared in our lab following the procedures described in previous publications.[32–33] Cetyltrimethylammonium bromide (CTAB, >99% purity) was purchased from Sigma Aldrich and used as received. Analytical grade KOH and HCl, purchased from Mallinckrodt, were used for pH modification. Sodium dodecyl sulfate (SDS, purity higher than 99%) was purchased from Fluka. Analytical grade KCl was purchased from Mallinckrodt.

Calcite and fluorite crystals used for surface force measurements were purchased from the Rockpick Legend Co., Salt Lake City, Utah. The crystals were clear and of optical quality. The crystallographic orientations of calcite and fluorite samples for the interfacial force measurements were, respectively, with the $(10\bar{1}4)$ and (111) planes exposed. The surface orientations of all crystal samples were determined from X-ray diffraction analysis. The surfaces for the interaction force measurements were cleaved just before experiments. The fluorite crystal used for streaming potential measurements was a FTIR window purchased from Pike Technologies, Inc. The surface roughness of this window was ~5 nm as measured by X-ray reflectivity (XRR).

Graphite particles were obtained from Lonza Inc. The diameter of these particles, determined using a dynamic light scattering technique, was found to be 1.0903 ± 0.303 μm. The pyrolytic graphite (HOPG) planar surface (35 mm × 20 mm × 2 mm) used in the streaming potential measurements was purchased from GE Advanced Ceramics.

The muscovite mica sheet was purchased from Alfa Aesar.

Flat plate steaming potential measurements (FPSP)

The theoretical and experimental details for streaming potential measurements using an asymmetric clamping cell can be found in the literature.[14–15] The zeta potential at a flat plate can be calculated from the following equation

$$\frac{\Delta U_s}{\Delta P} = \frac{\varepsilon\varepsilon_0}{\mu\kappa}\left(\frac{\zeta_{ref} + \zeta_{sample}}{2}\right) = \frac{\varepsilon\varepsilon_0}{\mu\kappa}\zeta_{avg} \qquad (1)$$

ζ_{ref} and ζ_{sample} are the zeta potentials at the PMMA reference and test sample surfaces, respectively, ΔU_s is the streaming potential, ΔP is the applied pressure, μ is the dynamic viscosity of the solution, ε_0 is the permittivity of free space, ε is the dielectric constant of the solution, κ is the solution conductivity. The zeta potential of the reference PMMA surface, ζ_{ref}, was measured first. Then the average potential of reference and sample surfaces, ζ_{avg}, was measured. Finally, the zeta potential of the test sample surface, ζ_{sample}, was calculated by the following equation:

$$\zeta_{sample} = 2\zeta_{avg} - \zeta_{ref} \qquad (2)$$

The asymmetric clamping cell to measure the streaming potential of flat substrates was purchased from Anton Paar, Graz, Austria. The clamping cell was attached to a commercial streaming potential analyzer (EKA, Brookhaven Instruments). The background electrolyte used was 1 mM KCl for the measurements when the concentration of KCl was not specified. Before each measurement, the cell was flushed in each direction four times. The surface of the plate was equilibrated with solution for about 20 min. Before the measurements, the pH, conductivity and electrode potential were calibrated carefully. Macroscopic bubbles were also meticulously removed from the apparatus. The potential *vs.* pressure curves were shown to have good linearity. All streaming potentials were measured using a pressure ramp mode from 0–300 mbar.

There are basically two operating modes for the measurement of streaming potential: constant pressure and ramp pressure. In this research, the constant pressure mode and ramp pressure mode have been compared and no significant difference in the streaming potential results was observed.

AFM soft contact imaging

Images were captured using a Nanoscope IIIA atomic force microscope (Digital Instruments) using standard silicon nitride cantilevers (Digital Instruments) with a spring constant of 0.12 N m^{-1}. Prior to imaging all cantilevers were cleaned by exposing them to UV light for 5 to 15 min. Images presented are deflection images showing the error in the feedback signal, with the integral and proportional gains set around 0.5 and scan rates of about 12 Hz. Images are presented as obtained and no filtering was performed except that inherent in the feedback loop. The substrates were left in contact with the solutions of interest for 30 min prior to imaging. All measurements were performed at a temperature of 23 ± 2 °C and the laser used for detecting the cantilever deflection was found to have a minimal effect on the temperature of the sample under the cantilever.

Interfacial force measurements

The interfacial force measurements were performed using a Nanoscope III atomic force microscope (AFM) from Digital Instruments Inc. All measurements were performed in a fluid cell using freshly prepared solutions and freshly cleaved mineral surfaces of about 10 mm in size. The triangular shaped cantilevers used in this research had a spring constant 0.58 N m^{-1}, and were purchased from Digital Instruments.

Spherical colloidal probes were fashioned on the tip of the cantilevers using an optical microscope and micromanipulation by the method of Ducker *et al.*[34] The attachment was performed one day prior to the interfacial force measurements. The interfacial forces were measured using contact mode. A deflection of the cantilever relates to the forces acting between the glued particle and the mineral surface. The range of cantilever deflection is monitored by the laser-photodiode system. Because the spring constant of the cantilever is known, the deflection can be converted to a force value. After interfacial force measurements the cantilever with attached sphere was taken for SEM imaging. The diameters of these spheres were measured from the SEM images. The force values in this research were normalized by the sphere radius.

Microelectrophoretic measurements (MEP)

Electrophoretic mobilities of the graphite particles and fluorite particles were measured using a Brookhaven ZetaPALS apparatus using the *Phase Analysis Light Scattering technique (PALS)* to determine the electrophoretic mobility of charged particles. The PALS technique does not require the application of large electric fields which may result in thermal problems since in the measurement of phase change the particle needs to move only a fraction of its own diameter for good results. The velocities of the charged particles are measured and the electrophoretic mobility is determined by dividing the measured velocity by the electric field strength applied. Before measurements, the solid particles were equilibrated in surfactant solutions. Six consecutive measurements were taken for each sample at room temperature and averaged.

Results and discussion

Validation of the streaming potential measurement procedure

This research uses the novel asymmetric clamping cell for the streaming potential measurements as described in the Experimental section. The zeta potentials at reference PMMA surfaces and at mica surfaces in the presence of dodecyltrimethylammonium bromide (DTAB) were first calculated based on streaming potential measurements. The curve for the zeta potential as a function of pH at the PMMA reference surface is quite similar to that reported in the

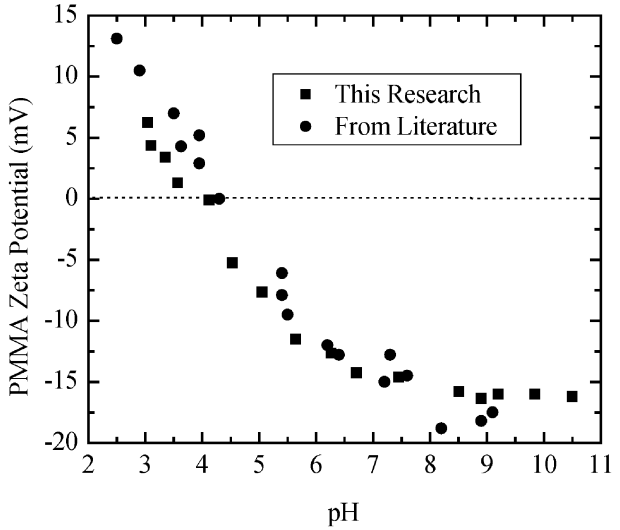

Fig. 1 Zeta potentials for PMMA reference surface measured in this research and reported in the literature as a function of solution pH. The concentration of background electrolyte KCl was 10 mM.

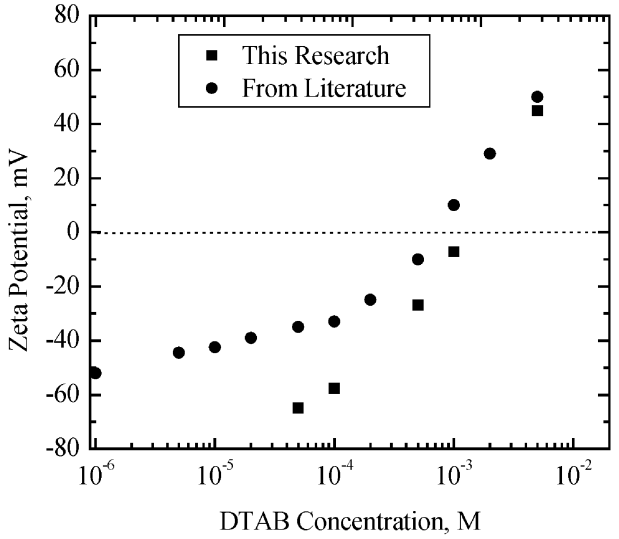

Fig. 2 Comparison of zeta potentials at muscovite mica surfaces as a function of the dodecyltrimethylammonium bromide (DTAB) concentration measured in the current research with those reported in the literature.[35]

literature.[14] See Fig. 1. For the DTAB/mica system, the zeta potential reversal has been observed at almost the same DTAB concentration as reported using the traditional streaming potential cell (rectangular) and experimental procedure,[35] which is shown in Fig. 2. The slight difference in the zeta potential curves in Fig. 2 is attributed to the different electrolyte solution and variation of the mica surface used in the current research. The validation of this new streaming potential measurement procedure has also been confirmed by agreement of the zeta potential at the surface of the NF-70 membrane obtained using asymmetric clamping cell with results obtained using the traditional rectangular cell as reported in the literature.[14]

The validation of this new streaming potential measurement procedure has also been extended to other systems in this research. A summary is presented in Table 1. From Table 1, a good agreement was established, giving confidence in the current technique.

Zeta-potential of surface micelles adsorbed at graphite surfaces

It is reported that the solution c.m.c is about 0.9 mM for CTAB and 8 mM for SDS.[43–44] The direct AFM images in Fig. 3 show that hemicylindrical micelles are formed at concentrations below their c.m.c at the graphite surface. At these surfactant concentrations the zeta potential of the graphite surface does not significantly change with change in concentration as shown in Fig. 4, corresponding well with surface micelle formation at the graphite surfaces. For both cationic and anionic surfactants, the AFM images show the adsorbed surfactant structures as hemicylindrical surface micelles although this graphite surface is negatively charged as presented in Table 1. Similar structures were identified for SDS by Wanless and Ducker.[45] From the fact that the surfactants form similar micellar structures at the negatively charged graphite surface irrespective of the charge on the surfactant head group, it is concluded that adsorption is mainly due to the van der Waals interaction and/or hydrophobic attraction between the nonpolar graphite surface and the hydrophobic alkyl chain of the surfactant molecules while the electrostatic interaction between the graphite and surfactant molecules plays a non-dominant role in the micellar formation. Adsorption at the planar graphite surface occurs in the form of hemicylindrical micelles, where the adsorbed hydrocarbon chains lie down on the graphite surface.

Since these hemicylindrical micelle structures of SDS and CTAB are formed at graphite surfaces, zeta potentials of the micelle covered graphite surface should represent the zeta-potential of the surface micelles. Both the streaming potential and electrophoretic measurements show that the zeta-potentials for SDS and CTAB surface micelles at the graphite surface are about −80 and +70 mV, respectively. These zeta-potential values are very close to the available data reported in the literature for micelles formed in the bulk solution phase.[46–50] Also it is found that the zeta potentials calculated from streaming potential measurements in the presence of CTAB agree well with the zeta potentials obtained from the electrophoretic mobility measurements.

Table 1 The signs of zeta potentials at neutral pH and various surfaces determined in this research using the FPSP procedure and compared with values reported in the literature using MEP and SP

System	FPSP	MEP	SP
Calcite	Negative and small[a]	Negative but small[36]	
Mica/Water	Negative[a]	Negative[37]	Negative[38]
Mica/DTAB	From negative to positive[a]		From negative to positive[35]
Si/SiO_2	Negative[a]	Negative[39,40]	
Graphite HOPG	Negative[a]	Negative[a]	
PMMA	Negative[a]		Negative[14]
Alumina	Positive[a]	Positive[41]	Positive[42]
NF-70 Membrane	Negative[14]		Negative[14]

[a] This research.

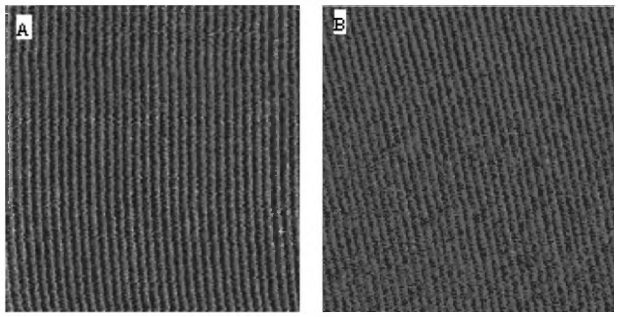

Fig. 3 AFM images (200 nm × 200 nm) showing the surface micelles on planar HOPG graphite surfaces in 6 mM SDS (image A) and 0.5 mM CTAB (image B) solutions at pH (5.3–5.8) and temperature 23 °C.

Adsorption of amine surfactants at the muscovite mica–water interface

Muscovite mica is an aluminosilicate mineral of layered structure as shown in Fig. 5. The bases of the tetrahedra are symmetrically opposed so that two opposite hexagonal rings outline a large cavity into which a potassium atom is situated with twelve-fold coordination. The potassium ions are used to neutralize the negatively charged sheets due to substitution for some of the Si^{4+} within the silica tetrahedra. When muscovite is cleaved, the surface of the sheet carries a fixed or constant negative charge that essentially depends only on the degree of Al/Si substitution in the silica tetrahedra. The zeta potential at the muscovite surface is shown in Fig. 6a as a function of pH. A constant zeta potential is observed in the pH range examined. The zeta potential of mica as a function of the cationic amine surfactant concentration in the presence of 1 mM KCl as background electrolyte at neutral pH is shown in Fig. 6b. A point of zeta reversal or PZR is observed for both DTAB and CTAB. The zeta potential becomes zero at a concentration defined as the point of zeta reversal. The zeta reversal phenomena observed indicates the adsorption of cationic surfactant molecules at the negatively charged mica surface. The PZR for CTAB is shifted to a lower concentration than that for DTAB. This behaviour is in agreement with the reported observation for pyridinium compounds of different chain length adsorbed by AgI sols[51] and observation for tetraalkylammonium ions adsorbed at negatively charged AgI.[52] The PZR moves to higher concentration in the presence of surface active surfactants with a decrease in chain length, which opposes the prediction made by S. Nishimura *et al.* that the PZR moves

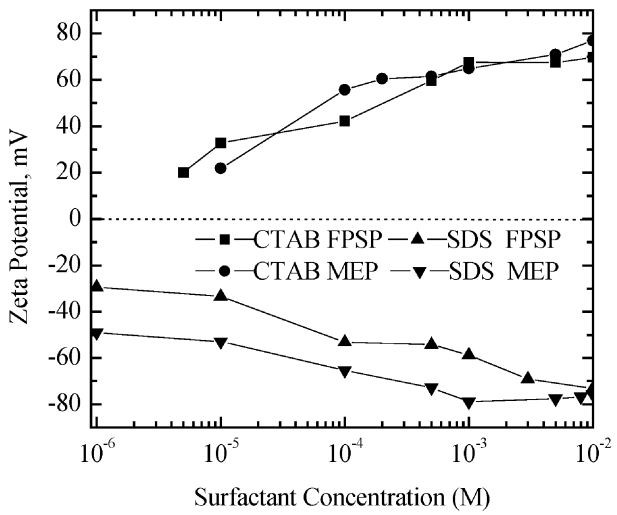

Fig. 4 Comparison of zeta potentials at graphite HOPG surface with those at graphite particles in the presence of CTAB and SDS at neutral pH.

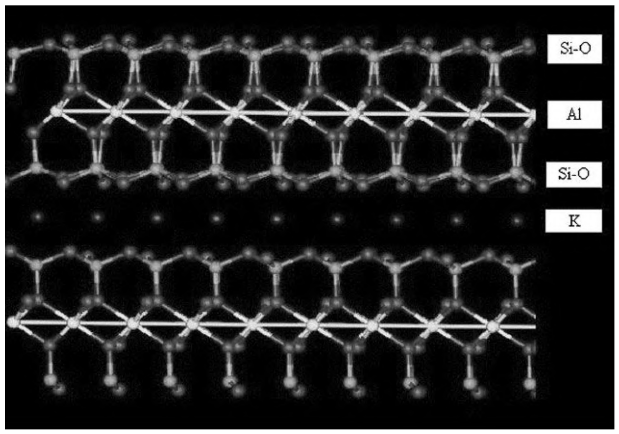

Fig. 5 Muscovite structures.

to higher concentration with an increase in length of the hydrocarbon chain.[35] Direct AFM images in Fig. 7 show that cationic surfactant molecules form micelles at the atomically smooth mica surface. The surface c.m.c for CTAB is also shown to be smaller than that for DTAB. This is consistent with the common knowledge about surfactant behavior in the bulk and at surfaces. Long chain surfactants are of lower c.m.c values when compared to short chain surfactants. They form

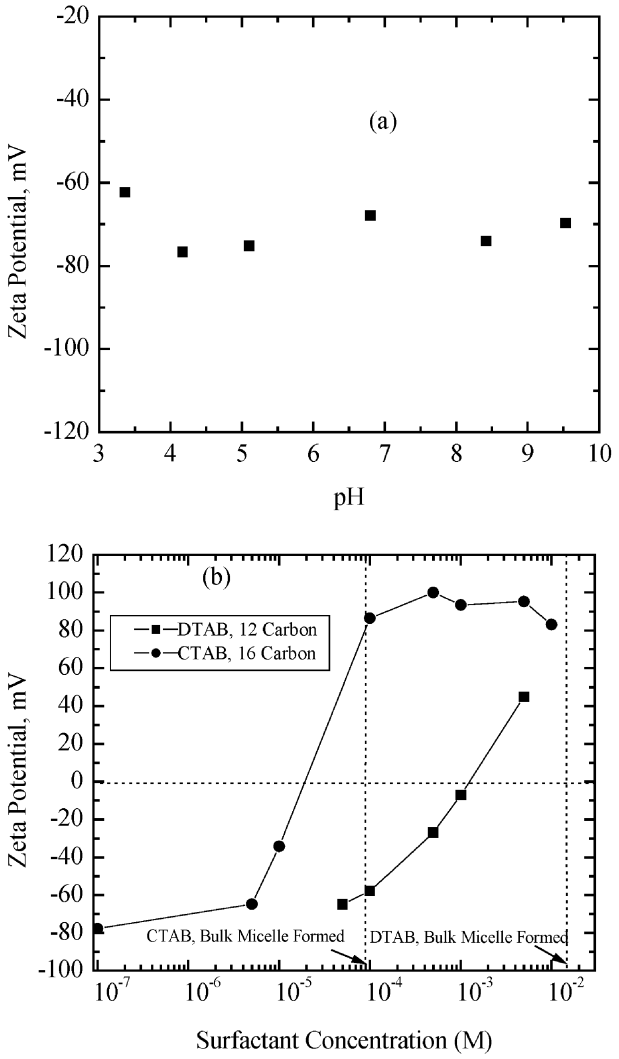

Fig. 6 Zeta potentials at mica surfaces in the absence of surfactants (a) and in the presence of surfactants (b). The background electrolyte solution, 1 mM KCl aqueous solution, is used for all the measurements.

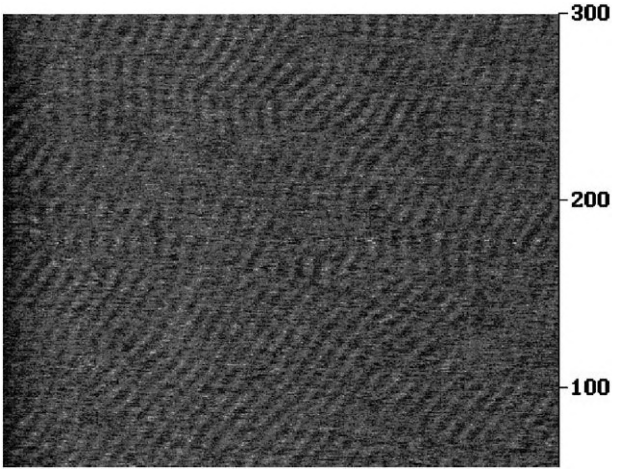

Fig. 7 Micellar structures of CTAB at mica surfaces.

molecular aggregates more easily. Fig. 7 shows the micellar structure at mica surfaces for CTAB. For CTAB, at 0.1 mM, the meandering linear structures are believed to be the cylindrical surface micelles. While for DTAB, it was reported that the c.m.c is about 15 mM[53] and at a concentration of 20 mM a micellar structure similar to Fig. 7 was observed by Ducker.[54]

Since SDS bears a negatively charged head group it should be Coulombically unfavorable for adsorption at the negatively charged surface of mica. Accordingly, no adsorbate structure was observed at the mica surface for SDS. This confirms the significance of electrostatic interaction for the adsorption of ionic surfactants at charged interfaces. As well, it suggests that Coulombic interactions play a pivotal role in the manifestation and adherence of adsorbed self-assembled cationic surfactant structures at the muscovite mica–solution interface.

Interaction forces between collector colloids and semi-soluble salt mineral surfaces

One research area of importance that has received little attention is the consideration of insoluble collector colloids and their significance in the flotation of semi-soluble salt minerals such as fluorite, calcite, apatite, *etc.*[55] In the case of calcium semi-soluble minerals and their flotation with oleate, formation of the calcium dioleate collector colloid must be considered.[56] In this research, calcium dioleate spheres have been prepared and used as probes to measure interaction forces between the calcium dioleate sphere and calcite/fluorite mineral surfaces. The forces curves are shown in Fig. 8.

The force curves in Fig. 8 can be divided into three regions. At large separation distances weak or no forces act between the probe and the surface, and no deflection of the cantilever is experienced. When the probe is brought closer to the surface, the cantilever bends to or deflects away from the surface depending on the attractive or repulsive force between the probe and the surface. The probe contacts with the surface when a linear increase of force is observed with a decrease in the separation distance (at $\sim$3 nm in Fig. 8a and $\sim$5 nm in Fig. 8b).

First of all, it is important to note that interaction forces are measured under non-equilibrium conditions in this research. During the force measurement experiments, the spherical calcium dioleate colloidal probe will experience some degree of dissociation or dissolution. Although force measurements were conducted about 10 min after the first approach, it was unlikely that the system reached equilibrium because the dissociation or dissolution of calcium dioleate and the mineral surfaces is a slow process.

A long-range repulsive force was observed in Fig. 8a between calcium dioleate and the $(10\bar{1}4)$ calcite surface at pH 8.1.

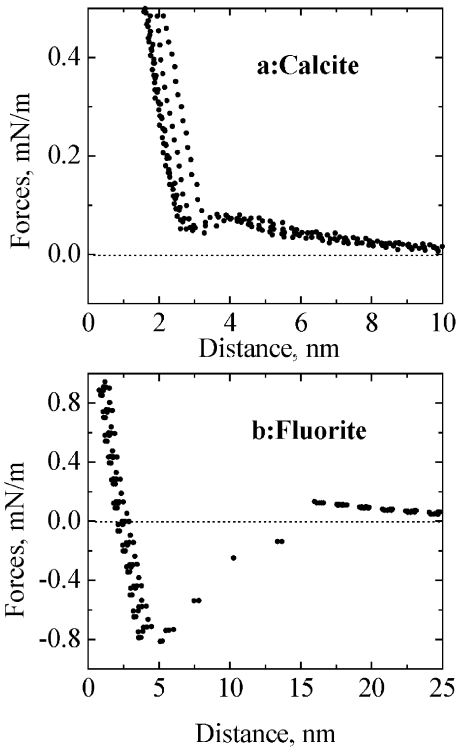

Fig. 8 Interaction forces between calcium dioleate spheres and calcite/fluorite surfaces at solution pH 8.1.

At short separation distances (around 5 nm) an attractive force component can be distinguished. After jump to contact, an elastic deformation of the spherical particle can be observed at a separation distance of 4.0 nm. Fig. 8b shows the normalized interfacial force *versus* distance curves measured between the calcium dioleate sphere and the (111) fluorite surface in water at solution pH 8.1. Repulsive forces are not great. It is evident that there is a strong attractive interaction of the calcium dioleate with the fluorite surface, an attraction which is much stronger than that observed at the calcite surface. Specifically, attractive forces at distances from 15 nm are evident.

To understand the interaction between calcium dioleate and mineral surfaces, it is necessary to identify the individual force components involved in the overall interaction. The surface charge must be considered in order to explain these interfacial forces. The calcium dioleate is negatively charged in water.[56] The zeta potentials at the calcite surface are small and, for the most part, are negative in the alkaline region.[56] The magnitude of the zeta potential becomes greater with an increase in pH. This result is in agreement with recently reported zeta potentials for calcite particles measured under well-controlled conditions.[36] Based on streaming potential measurements at the $(10\bar{1}4)$ calcite surface, it can be concluded that the repulsive interfacial forces measured using the AFM colloidal probe technique are a result of opposing electrical double layers. A local minimum in the force/radius *vs.* distance curve can be attributed to attractive van der Waals forces.

The same explanation can be applied to the interfacial force curve measured between calcium dioleate and the (111) fluorite surface. The electrical double layer repulsion can be seen at distances of 20 nm. Due to the non-equilibration state of the system, the (111) fluorite surface is still negatively charged as shown in Fig. 9. This result at the (111) fluorite surface at non-equilibrate state is quite different from the zeta potential for particles measured using the microelectrophoresis technique. The zeta potential for fluorite particles at a solid concentration of 40 mg per 100 ml water shows a positive sign. As reported from low energy electron diffraction study and AFM evidence, the exposed top layer at the (111) fluorite surface is the fluorine

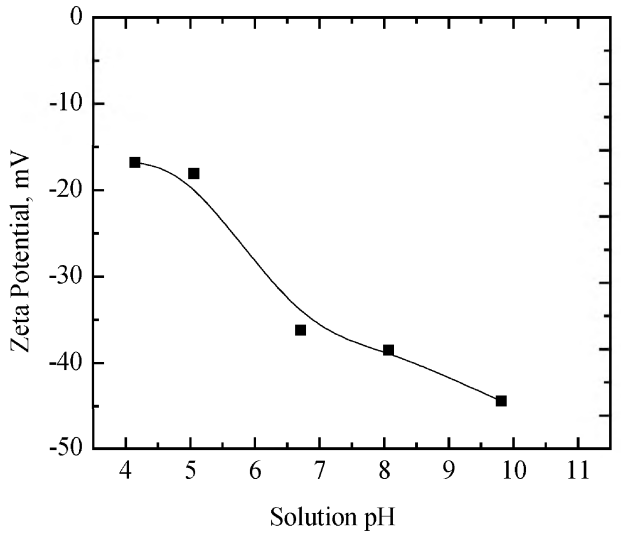

Fig. 9 Zeta potential at the (111) fluorite surface as a function of solution pH.

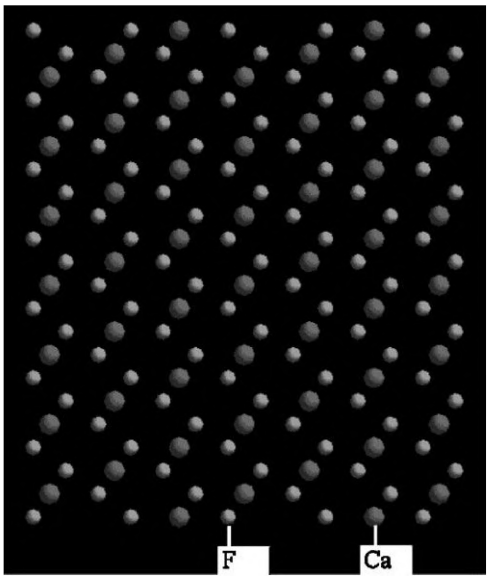

Fig. 10 Graphic representative of fluorite (111) surface along the direction from left to right. The top most atoms at (111) surface are fluorine atom layer (light grey). The spacing between the two adjacent F^{-}–Ca^{2+}–F^{-} triple layers is 3.154 Å.

atoms as shown in Fig. 10. It is reasonable that under non equilibrium conditions zeta potentials at the (111) fluorite surface are negative in view of the (111) fluorite surface structure.

In the literature, the surface sensitive apparatus-sum frequency generation spectroscopy (SFG) was used to examine the interfacial structure in the proximity of fluorite surface. The reported PZC for fluorite surface was about pH 6.2 based on the analysis of SFG signal,[57] which is also quite different from the result presented in this paper and the majority of reported PZC values for fluorite particles (PZC is in the range pH 9.5 to pH 10.0). Because the authors have not examined the surface crystallographic plane of fluorite samples used in their SFG analysis, the conclusions and data derived from the analysis of SFG spectra could not be compared with our observations. The zeta potential is considered as a function of exposed surface properties under non equilibrium conditions. For fluorite surfaces, it should be regarded with caution because the dissolved cations and anions may also dramatically change the interfacial water structure upon dissolved ions entering the bulk from the surface. The OH peaks in the SFG spectra may be a function of the surface crystallographic plane and the degree of surface hydration.

After the repulsive component in the overall force curves is identified, the consequent analysis for the other interactions contributed to the overall interaction behavior becomes easier. The most important difference between calcite and fluorite is the presence of long-range attractive forces for fluorite which are stronger and extend further than the typical van der Waals attraction. These forces are usually called hydrophobic forces, and are reported in many systems between hydrophobic surfaces, and between one hydrophobic surface and another hydrophilic surface. These forces are usually explained by a water structure-related entropic effect and/or formation of submicroscopic bridging cavities between interacting surfaces.[58–60] A comparison of the magnitude and distance for attractive interaction found in this research with those for other hydrophobic interaction systems reported in the literature[59,61,62] is shown in Table 2.

A significant long-range attractive force is found existing between calcium dioleate and fluorite whereas only a very weak, short-range attraction is observed between calcium dioleate and calcite. This helps to explain the excellent flotation for fluorite but poor flotation response for calcite with the calcium dioleate collector colloid as reported in the literature.[63] This is also in agreement with contact angle measurements. Fluorite has been reported to have a contact angle of 10° to 30° while calcite has a contact angle of ~0°.[64,65]

Summary and conclusions

The zeta potentials at several flat mineral plates are calculated from the streaming potential measurements using a novel clamping cell. These zeta potential data are found very useful for explaining the interfacial phenomena involving the consideration of electric double layer interaction:

(1) For negatively charged HOPG graphite, both cationic and anionic surfactant can form "wormlike" micelle structure. This fact indicates that the van der Waals force and/or hydrophobic attractive between the hydrophobic HOPG surface and the surfactant hydrophobic alkyl chain plays a critical role for the micelle formation at HOPG template while the electrostatic interaction plays a non-dominant role.

(2) For the constant negatively charged mica surface, only cationic surfactants can form meandering micelle structures, which suggest that electrostatic attraction between the mica

Table 2 Comparison of the magnitude and distance of attractive interactions found in this research and those selected from the literature

Probe	Calcium dioletate	Glass sphere	Bare mica	Fluorocarbon
Surface	Fluorite	Silica	Hydrophobic mica	Fluorocarbon
Probe	CA*: 80°	CA*: 109°	Hydrophilic	CA*: 93°
Surface	Hydrophilic	CA*: 75°–109°	Hydrophobic	CA*: 93°
Magnitude/mN m^{-1}	0.8	5–20	Very strong	10–20
Distance/nm	10–35	>32	>100	80–90
Reference	This research	59	61	62

CA*: Contact Angle/°.

surface and surfactant head group is one of the driving forces for the formation of micelles. In this case, the surface template introduces and controls the phase and structure properties of the micellar structure.

(3) The zeta potential at one specific crystallographic plane is not always the same as the zeta potential measured for particle samples, especially under the non-equilibrium solution conditions. This observation is confirmed in this research and in the literature.

(4) The presence of strong attractive force observed in the interaction force curve between calcium dioleate and fluorite surface indicates that fluorite should have a better flotation response than calcite, which is in agreement with the flotation results reported in the literature.

Acknowledgements

This research was supported by the DOE Office of Basic Sciences (Grant No DE-FG-03-93-ER14315) and the National Science Foundation (INT-0227583, INT-0096920 and INT-0111248). Also, the authors acknowledge the financial and technical support from the Engineering Research Center (ERC) for Particle Science & Technology at the University of Florida, Gainesville, Florida.

References

1 R. J. Hunter, *Foundation of Colloid Science*, Oxford University Press, New York, 2001, 2nd edn., ch. 1.
2 L. Besra, D. K. Sengupta and S. K. Roy, *Int. J. Miner. Process.*, 2000, **59**, 89.
3 S. B. Johnson, G. V. Franks, P. J. Scales, D. V. Bogrer and T. W. Healy, *Int. J. Miner. Process.*, 2000, **58**, 267.
4 K. B. Quast and D. J. Readett, *Adv. Colloids Interface Sci.*, 1987, **17**, 169.
5 R. H. Yoon, T. Salman and G. Donnay, *J. Colloid Interface Sci.*, 1979, **70**, 483.
6 M. E. Labib, *Colloids Surf.*, 1988, **29**, 293.
7 P. L. De Bruyn and G. E. Agar, *Froth Flotation-50th Anniversary Volume*, ed. M. C. Fuerstenau, AIME, New York, 1962, p. 91.
8 F. F. Aplan and D. W. Fuerstenau, *Froth Flotation-50th Anniversary Volume*, ed. M. C. Fuerstenau, AIME, New York, 1962, p. 170.
9 H. van Olphen, *An Introduction to Clay Colloid Chemistry*, Interscience Publishers, New York, 1963, p. 90.
10 I. Iwasaki, S. R. B. Cooke and A. F. Colombo, *US Bureau of Mines, RI5593*, United States Department of the interior, 1960, 1.
11 I. Iwasaki, S. R. B. Cooke and H. S. Choi, *Trans. AIME*, 1960, **217**, 238.
12 I. Iwasaki, S. R. B. Cooke and Y. S. Kim, *Trans. AIME*, 1962, **241**, 453.
13 J. D. Miller and S. Veeramasuneni, in *Surfaces of Nanoparticles and Porous Materials*, ed. A. James Schwarz and I. Cristian, Contescu Marcel Dekker, Inc., 1999.
14 S. L. Walker, S. Bhattacharjee and E. M. V. Hoek, *Menachem Elimelech. Langmuir*, 2002, **18**, 2193.
15 A. E. Childress and M. Elimelech, *J. Membr. Sci.*, 1996, **119**, 253.
16 D. Erickson, D. Q. Li and C. Werner, *J. Colloid Interface Sci.*, 2000, **232**, 186.
17 C. Werner, R. Zimmermann and T. Kratzmuller, *Colloids Surf., A*, 2000, **192**, 205.
18 R. Scheiss, P. B. Welzel, C. Werner and W. Knoll, *Langumir*, 2001, **17**, 4304.
19 A. Sze, D. Erickson, L. Q. Ren and D. Q. Li, *J. Colloid Interface Sci.*, 2003, **261**, 402.
20 A. Yaroshchuk and V. Rititsch, *Langmuir*, 2002, **18**, 2036.
21 M. Sbai, A. Szymczykl, P. Fievet, A. Sorin, A. Vidonne, S. Pellet-Rostaing, A. Favre-Reguillon and M. Lemaire, *Langmuir*, 2003, **19**, 8867.
22 P. Fievet M. Sbai, A. Szymczyk and A. Vidonne, *J. Membr. Sci.*, 2003, **226**, 227.
23 R. J. Hunter, *Zeta Potential in Colloid Science, Principle and Applications*, Academic Press, London, 1981.
24 O. El-Gholabzour, M. A. Cabrerizo-Vilchez and R. Hidalgo-Alvarez, *J. Colloid Interface Sci.*, 2003, **261**, 386.
25 A. Szymcyk, P. Fievet and A. Foissy, *J. Colloid Interface Sci.*, 2002, **255**, 323.
26 R. Zimmermann, S. Dukhin and C. Werner, *J. Phys. Chem. B*, 2001, **105**, 8544.
27 H. J. Modi and D. W. Fuerstenau, *J. Phys. Chem.*, 1957, **61**, 640.
28 P. G. Hartley, I. Larson and P. J. Scales, *Langmuir*, 1997, **13**, 2207.
29 K. A. Becraft, F. G. Moore and G. L. Richmond, *J. Phys. Chem. B*, 2003, **107**, 3675.
30 L. D. Tichanen, M. Isabel Tejedor-Tejedor and M. A. Anderson, *Langmuir*, 1991, **7**, 451.
31 G. V. Franks and L. Meagher, *Colloids Surf., A*, 2003, **214**, 99.
32 J. Drelich, J. Nalaskowski and J. D. Miller, *J. Colloid Interface Sci.*, 1998, **201**, 253.
33 J. Nalaskowski, J. Drelich, J. Hupka and J. D. Miller, *J. Adhesion Sci. Technol.*, 1999, **13**, 1.
34 W. A. Ducker, T. J. Senden and R. M. Pashley, *Nature*, 1991, **353**, 239.
35 S. Nishimura, P. J. Scales, S. Biggs and T. W. Healy, *Langmuir*, 2000, **16**, 690.
36 P. Moulin and H. Roques, *J. Colloid Interface Sci.*, 2003, **261**, 115.
37 N. Debacher and R. H. Ottewill, *Colloids Surf., A*, 1992, **65**, 51.
38 M. Zembala and Z. Adamczyk, *Langmuir*, 2000, **16**, 1593.
39 M. Kosmulski and E. Matijević, *Langmuir*, 1992, **8**, 1060.
40 V. Nikolakis, M. Tsapatsis and D. G. Vlachos, *Langmuir*, 2003, **19**, 4619.
41 W. B. Samuel de Lint, N. E. Benes, J. Lyklema, H. J. M. Bouwmeester, A. J. van der Linde and M. Wessling, *Langmuir*, 2003, **19**, 5861.
42 S. Bhattacharjee, B. P. Singh and L. Besra, *J. Colloid Interface Sci.*, 2002, **254**, 95.
43 J. F. Liu and W. A. Ducker, *J. Phys. Chem. B*, 1999, **103**, 8558.
44 M. Baviere, B. Bazin and R. Aude, *J. Colloid Interface Sci.*, 1983, **92**, 580.
45 E. J. Wanless and W. A. Ducker, *J. Phys. Chem.*, 1996, **100**, 3207.
46 D. Stigter and K. J. Mysels, *J. Phys. Chem.*, 1955, **59**, 45.
47 P. H. Wiersema, A. L. Loeb and J. T. G. Overbeek, *J. Colloid Interface Sci.*, 1966, **22**, 78–99.
48 R. W. O'Brien and L. R. White, *J. Chem. Soc., Faraday Trans.*, 1978, **74**(2), 1607.
49 F. Tokiwa and K. Aigami, *Kolloid Z. Z. Polym.*, 1970, **239**, 687.
50 K. Kameyama and T. Takagi, *J. Colloid Interface Sci.*, 1990, **144**, 601.
51 R. H. Ottewill and M. C. Rastogi, *Trans. Faraday. Soc.*, 1960, **56**, 880.
52 A. de Keizer and J. Lyklema, *J. Colloid Interface Sci.*, 1980, **75**, 171.
53 N. M. Van Os, J. R. Haak and L. A. M. Rupert, *Physico-Chemical Properties of Selected Anionic, Cationic and Non-ionic Surfactants*, Elsevier, Amsterdam, 1993.
54 W. A. Ducker and E. J. Wanless, *Langmuir*, 1996, **12**, 5915.
55 J. D. Miller, in *Proceedings: Flotation and Flocculation from Fundamentals to Applications*, Hawaii, 2002.
56 K. Fa, T. Jiang, J. Jakub Nalaskowski and J. D. Miller, *Langmuir*, 2003, **19**, 10523.
57 K. A. Becraft and G. L. Richmond, *Langmuir*, 2001, **17**, 7721.
58 J. N. Israelachvili and R. M. Pashley, *J. Colloid Interface Sci.*, 1984, **98**, 500.
59 R.-H. Yoon, D. H. Flinn and Y. I. Rabinovich, *J. Colloid Interface Sci.*, 1997, **185**, 363.
60 J. L. Parker, P. M. Claesson and P. Attard, *J. Phys. Chem.*, 1994, **98**, 8468.
61 Per M. Claesson and H. K. Christenson, *J. Phys. Chem.*, 1988, **92**, 1650.
62 Yi-Hua. Tsao and D. Fennell Evans, *Langmuir*, 1993, **9**, 779.
63 E. W. Giesekke and P. J. Harris, in *Mintek 50: international conference on mineral science and technology*, Randburg, Council for Minerals Technology, 1984, **Vol. 1**, 269.
64 J. Drzymala, *Adv. Colloid Interface Sci.*, 1994, **50**, 143.
65 C. A. Young, PhD Thesis, University of Utah, 1995.

